




Biochemical and Genetic Analysis of the *Chlamydia* GroEL Chaperonins

Melissa Illingworth,^a Anna J. Hooppaw,^b Lu Ruan,^a  Derek J. Fisher,^b Lingling Chen^{a,c}

Department of Molecular and Cellular Biochemistry, Indiana University, Bloomington, Indiana, USA^a; Department of Microbiology, Southern Illinois University, Carbondale, Illinois, USA^b; Department of Chemistry, College of Chemistry and Chemical Engineering, Xiamen University, Xiamen, China^c

ABSTRACT Chaperonins are essential for cellular growth under normal and stressful conditions and consequently represent one of the most conserved and ancient protein classes. The paradigm *Escherichia coli* chaperonin, EcGroEL, and its cochaperonin, EcGroES, assist in the folding of proteins via an ATP-dependent mechanism. In addition to the presence of *groEL* and *groES* homologs, *groEL* paralogs are found in many bacteria, including pathogens, and have evolved poorly understood species-specific functions. *Chlamydia* spp., which are obligate intracellular bacteria, have reduced genomes that nonetheless contain three *groEL* genes, *Chlamydia groEL* (*ChgroEL*), *ChgroEL2*, and *ChgroEL3*. We hypothesized that ChGroEL is the bona fide chaperonin and that the paralogs perform novel *Chlamydia*-specific functions. To test our hypothesis, we investigated the biochemical properties of ChGroEL and its cochaperonin, ChGroES, and queried the *in vivo* essentiality of the three *ChgroEL* genes through targeted mutagenesis in *Chlamydia trachomatis*. ChGroEL hydrolyzed ATP at a rate 25% of that of EcGroEL and bound with high affinity to ChGroES, and the ChGroEL-ChGroES complex could refold malate dehydrogenase (MDH). The chlamydial ChGroEL was selective for its cognate cochaperonin, ChGroES, while EcGroEL could function with both EcGroES and ChGroES. A P35T ChGroES mutant (ChGroESP35T) reduced ChGroEL-ChGroES interactions and MDH folding activities but was tolerated by EcGroEL. Both ChGroEL-ChGroES and EcGroEL-ChGroESP35T could complement an EcGroEL-EcGroES mutant. Finally, we successfully inactivated both paralogs but not *ChgroEL*, leading to minor growth defects in cell culture that were not exacerbated by heat stress. Collectively, our results support novel functions for the paralogs and solidify ChGroEL as a bona fide chaperonin that is biochemically distinct from EcGroEL.

IMPORTANCE *Chlamydia* is an important cause of human diseases, including pneumonia, sexually transmitted infections, and trachoma. The chlamydial chaperonin ChGroEL and chaperonin paralog ChGroEL2 have been associated with survival under stress conditions, and ChGroEL is linked with immunopathology elicited by chlamydial infections. However, their exact roles in bacterial survival and disease remain unclear. Our results further substantiate the hypotheses that ChGroEL is the primary chlamydial chaperonin and that the paralogs play specialized roles during infection. Furthermore, ChGroEL and the mitochondrial GroEL only functioned with their cochaperonin, in contrast to the promiscuous nature of GroEL from *E. coli* and *Helicobacter pylori*, which might indicate a divergent evolution of GroEL during the transition from a free-living organism to an obligate intracellular lifestyle.

KEYWORDS *Chlamydia*, GroEL, GroES, Hsp60, chaperonin

Chaperonins (Hsp60s) and cochaperonins (Hsp10s) are essential molecular chaperones that mediate protein folding under both normal and stress conditions and are conserved among the three domains of life (1, 2). The detailed molecular mechanism

Received 8 December 2016 Accepted 1 April 2017

Accepted manuscript posted online 10 April 2017

Citation Illingworth M, Hooppaw AJ, Ruan L, Fisher DJ, Chen L. 2017. Biochemical and genetic analysis of the *Chlamydia* GroEL chaperonins. *J Bacteriol* 199:e00844-16. <https://doi.org/10.1128/JB.00844-16>.

Editor Richard L. Gourse, University of Wisconsin—Madison

Copyright © 2017 American Society for Microbiology. All Rights Reserved.

Address correspondence to Derek J. Fisher, fisher@micro.siu.edu, or Lingling Chen, linchen@indiana.edu.

of this chaperonin system has been revealed from intensive biochemical and structural studies of the *Escherichia coli* GroEL and GroES system (3–6). *E. coli* GroEL (EcGroEL) is a tetradecamer assembled from two heptameric rings stacked back-to-back, forming two functionally correlated cavities for binding and folding of the misfolded substrate protein (7). Each EcGroEL monomer folds into three domains. (i) The apical domain is located at the opening of the folding cavity and contains the binding sites for the misfolded substrate protein and EcGroES. (ii) The equatorial domain forms the bottom of the folding cavity, comprises all the inter-ring and most of the intra-ring contacts, and contains the nucleotide binding site. (iii) The intermediate domain connects the apical and equatorial domains, transmitting the signal between them. The cochaperonin, EcGroES, functions as a heptamer (8, 9) in which amino acids 17 to 35 form a structurally flexible region, termed the mobile loop, that is important for GroES–GroEL interactions. In the EcGroEL–EcGroES–ADP (10) crystal structure, the amino acids $I_{25}V_{26}L_{27}$ of EcGroES make direct contact with EcGroEL, mediated largely by hydrophobic interactions. Overall, the system functions as a barrel in which EcGroES binds to one end of the heptameric EcGroEL ring, inducing a large domain movement in EcGroEL and leading to the formation of an enclosed cavity where protein folding occurs.

Besides the conventional folding chaperonin, many bacteria contain multiple GroEL paralogs (11, 12). Mycobacteria, including *Mycobacterium tuberculosis*, contain extra chaperonin copies (13, 14) that play important roles in granuloma formation (15), biofilm maturation (16), and cell wall synthesis and oxidative stress resistance (17). Since *groEL* is among the few ancient genes that are essential and conserved across the three domains of life (1, 2), it has been proposed that bacteria have evolved a mechanism to duplicate *groEL* and repurpose these paralogs for specialized functions important for individual survival (12).

Chlamydia can cause a range of respiratory, ocular, and sexually transmitted infections (STIs), the last of which is the most common CDC-reportable bacterial infection in the United States (18). *Chlamydia* is an obligate intracellular Gram-negative bacterium that undergoes a two-phase developmental cycle (19) comprised of the extracellular infectious elementary body (EB) and the intracellular noninfectious replicative reticulate body (RB). *Chlamydia* possesses a relatively small genome of ~1.0 Mb (~900 open reading frames [ORFs]) that is hypothesized to have reached a stable point in genome reduction, i.e., that which remains likely plays an important role in some stage of development, growth, and/or pathogenesis (20, 21). Strikingly, its reduced genome encodes three chaperonins, termed ChGroEL, ChGroEL2, and ChGroEL3. Sequence identity between ChGroEL and EcGroEL is high (64%), while that between ChGroEL2 or ChGroEL3 and EcGroEL is low (23% or 32%, respectively). Previous research found that ChGroEL–ChGroES assists in the folding of proteins, including malate dehydrogenase (MDH) (22), and can replace EcGroEL–EcGroES to support the growth of *E. coli* (23), suggesting a conventional folding chaperone function for ChGroEL. By contrast, ChGroEL2 and ChGroEL3 cannot substitute for EcGroEL (23), suggesting that neither paralog duplicates the conventional folding function of a chaperonin.

We (and others) have hypothesized that *Chlamydia*'s lifestyle as an obligate intracellular pathogen with a biphasic developmental cycle imposes a unique selection environment resulting in novel biochemical properties of ChGroEL and the repurposing of the chaperonin paralogs, ChGroEL2 and ChGroEL3, to fulfill pathogen-specific needs. To further investigate the roles of the chaperonins in *Chlamydia*, we characterized ChGroEL–ChGroES *in vitro* and *in vivo* using *E. coli* as a surrogate host and found that the biochemical properties of ChGroEL are distinct from those of EcGroEL. In addition, we demonstrated through the creation of intron-based insertional mutants in *C. trachomatis* that *ChgroEL2* and *ChgroEL3* are not essential for growth in cell culture under normal and heat-induced stress conditions. Our results further support ChGroEL as the bona fide GroEL homolog in *Chlamydia* and set the stage to further elucidate the biochemical properties and substrate preferences of chaperonins and the unique roles of the chlamydial chaperonin paralogs.

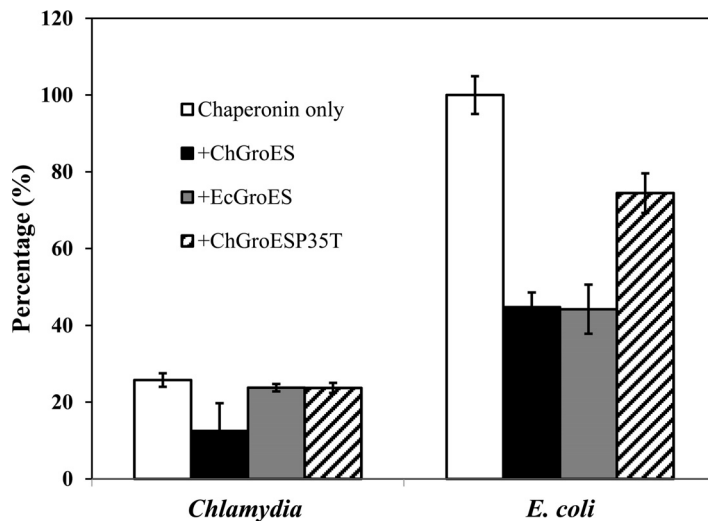


FIG 1 ATP hydrolysis activities of chaperonins alone or in the presence of cochaperonins. The ATP hydrolysis rate of EcGroEL was set to 100%. All the rates are listed in Table 1. Error bars represent standard deviations from at least three measurements. ATP hydrolysis was assayed using the malachite green method.

RESULTS

ATP hydrolysis of ChGroEL. We initially sought to thoroughly characterize the biochemical properties of ChGroEL to perhaps explain why additional chaperonins are encoded by the genome of *Chlamydia*. ChGroEL hydrolyzed ATP at a rate 25% of that of EcGroEL (Fig. 1 and Table 1). A prior study with ChGroEL from *C. pneumoniae* reported ATP hydrolysis at a rate 50% of that of EcGroEL (22). ChGroES inhibited the ATPase activity of ChGroEL by 50%, the same inhibitory effect seen for EcGroES with EcGroEL (24–28). Inhibition of ChGroEL was not observed using EcGroES, suggesting that no direct interaction between the chlamydial chaperonin and the *E. coli* cochaperonin occurred. Intriguingly, ChGroES decreased ATP hydrolysis by EcGroEL to the same level (50%) as that by the cognate EcGroES (Table 1). These findings suggest that the chlamydial chaperonin is selective for its cognate cochaperonin but that the *E. coli* chaperonin is promiscuous and can collaborate with cochaperonin homologs.

The cochaperonin interacts with the chaperonin via a mobile loop that contains the conserved tripeptide binding site amino acids I₂₅V₂₆L₂₇ (EcGroES numbering) (10). The residues following the binding site are Thr for EcGroES and Pro for ChGroES (see Fig. S1 in the supplemental material). Since structural dynamics of the mobile loop are important for a cochaperonin-chaperonin interaction (29) and the constrained side chain of Pro is likely to affect these dynamics, we mutated Pro to Thr in ChGroES,

TABLE 1 Biochemical characterizations of the chaperonin systems from *Chlamydia* and *E. coli*

Sample	ATPase activity (mol/min) (mean [SD])	MDH yield ^a (%)	K _d ^b (nM) (mean [SD])
ChGroEL	0.095 (0.007)	NA ^c	NA
ChGroEL + ChGroES	0.046 (0.005)	53.9	40.0 (10.7)
ChGroEL + EcGroES	0.088 (0.027)	15.8	ND ^d
ChGroEL + ChGroESP35T	0.087 (0.005)	10.1	ND
EcGroEL	0.368 (0.018)	NA	NA
EcGroEL + EcGroES	0.163 (0.014)	60.9	6.0 (0.6)
EcGroEL + ChGroES	0.165 (0.024)	51.6	8.8 (0.6)
EcGroEL + ChGroESP35T	0.274 (0.019)	34.4	563.0 (39.0)

^aAveraged over the last two time points (45 and 60 min).

^bBinding affinity.

^cNA, not available.

^dND, not detected.

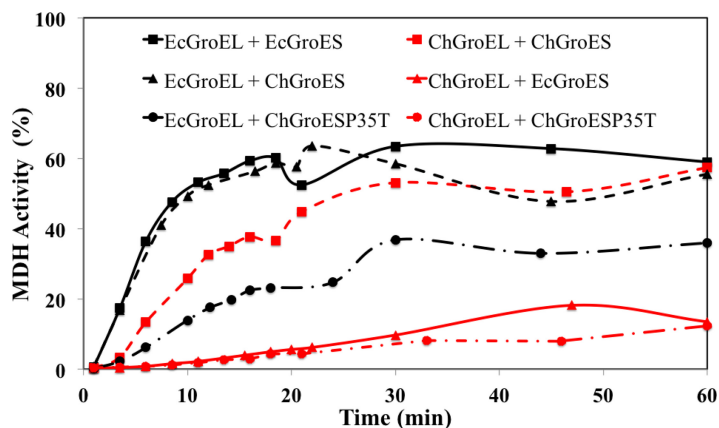


FIG 2 Folding of MDH by the chaperonin systems. Black lines, samples containing chaperonin EcGroEL; red lines, samples containing ChGroEL. MDH activity was evaluated via its enzymatic reduction of mesoxalic acid using electrons from NADH. Representative results from 3 experiments are shown. The average folding yields of MDH are listed in Table 1.

creating ChGroESP35T. In the presence of ChGroESP35T, ChGroEL largely maintained its ATPase activity (92.3% of that of wild-type ChGroEL) (Fig. 1), indicating that the P35T mutation abolished the binding of ChGroES to ChGroEL. The mutation also weakened binding to EcGroEL (Fig. 1), as ChGroESP35T exerted a lesser degree of inhibition (25%) than ChGroES on the ATPase activity of EcGroEL. These findings suggest an important role for P35 in the interaction of ChGroES with ChGroEL.

Folding activity of ChGroEL-ChGroES. We next investigated the activity of the chlamydial chaperonin system in assisting the folding of malate dehydrogenase (MDH). Spontaneous folding of MDH is low, and efficient folding of MDH requires the complete chaperonin system, including chaperonin, cochaperonin, and ATP (30). ChGroEL-ChGroES refolded MDH but with slower kinetics than EcGroEL-EcGroES (Fig. 2). The slow MDH folding kinetics of the chlamydial chaperonin system may be correlated with its low ATP hydrolysis rate (Fig. 1). No active MDH folding was observed using ChGroEL-EcGroES, while the high MDH folding efficiency of EcGroEL-EcGroES was maintained with EcGroEL-ChGroES (Fig. 2). These findings, consistent with those from the ATPase experiments, indicate that ChGroEL is selective for its cognate cochaperonin in contrast to EcGroEL's cochaperonin promiscuity.

The P35T mutation in ChGroES led to a loss of MDH folding activity when paired with ChGroEL. Since folding of MDH requires an enclosed chaperonin folding cavity, the lack of efficient MDH folding suggested no formation of ChGroEL-ChGroESP35T, supporting the importance of P35 for interactions between ChGroES and ChGroEL. The P35T mutation also impacted the folding activity of EcGroEL-ChGroES, as it lowered the MDH folding rate and reduced the folding yield by 50% compared with that of the wild-type ChGroEL (Fig. 2).

Binding affinity between chaperonin and cochaperonin. Since formation of the enclosed chaperonin cavity is required for chaperone function, we measured the binding affinity between chaperonin and cochaperonin using microscale thermophoresis (MST) (Fig. 3). In the presence of ADP, the EcGroEL-EcGroES interaction is tight, with a dissociation constant (K_d) of 6.0 ± 0.6 nM, consistent with the values reported by other techniques (26, 31, 32). The ChGroEL-ChGroES interaction is approximately six times weaker, with a K_d of 40.0 ± 10.7 nM.

ChGroEL displayed no affinity for EcGroES under the experimental conditions ($K_d > 11 \mu\text{M}$) (data not shown in Fig. 3). The lack of a ChGroEL-EcGroES interaction is consistent with the lack of inhibition of ChGroEL's ATPase activity by EcGroES and the lack of MDH folding activity by ChGroEL-EcGroES. By contrast, EcGroEL interacted with ChGroES with the same binding affinity with which it interacted with the cognate EcGroES. ChGroES and EcGroES had similar binding affinities for EcGroEL (Table 1),

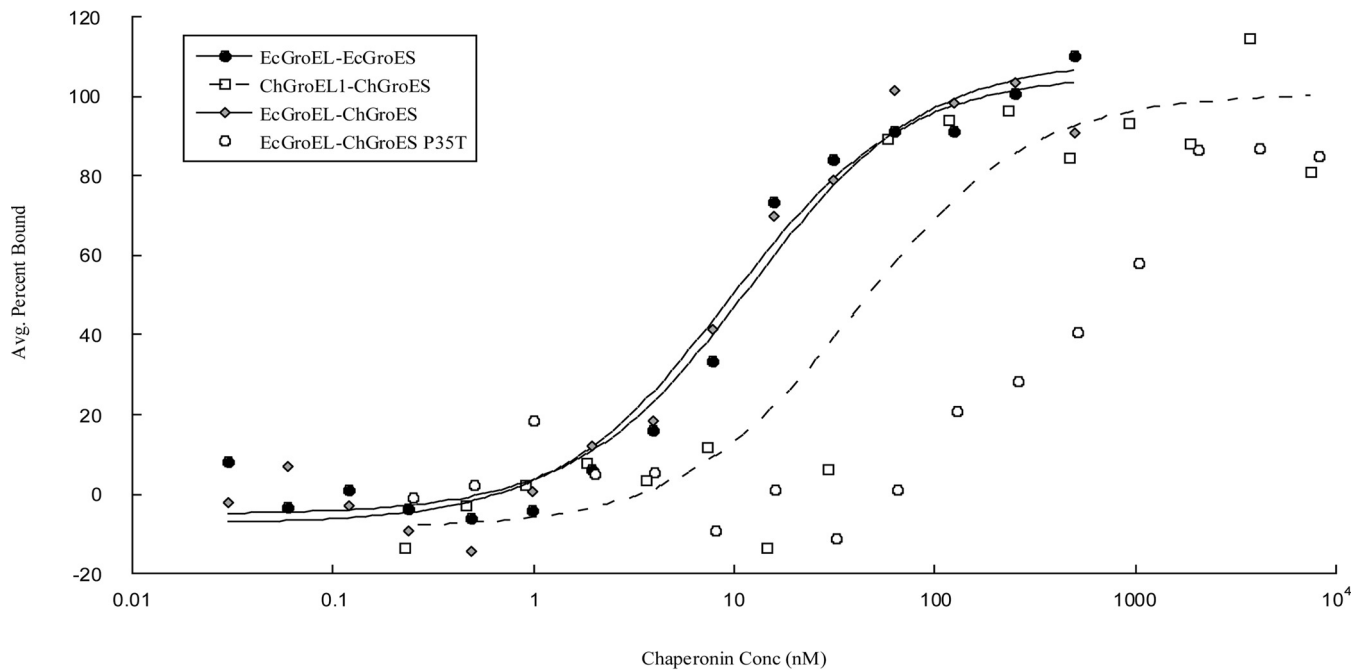


FIG 3 Chaperonin-cochaperonin interaction affinities by MST. Labeled cochaperonins were kept at a constant concentration of 10 nM while unlabeled EcGroEL or ChGroEL was titrated. To obtain the percentage bound, the value of the bottom plateau of the curve was subtracted from each raw fluorescence value and the result was divided by the amplitude. Data for each sample were fit to the equation $y = [m_1 + (m_2 - m_1)/(1 + m_3/x)]$ to generate the titration line and to derive the dissociation constant (K_d). The derived K_d values are summarized in Table 1.

corroborating the ability of both cochaperonins to inhibit EcGroEL's ATPase activity and promote the folding of MDH (Fig. 1 and 2). These findings indicate that ChGroEL has a stringent selectivity for its cognate ChGroES but that EcGroEL can accommodate cochaperonins of different sources.

The P35T mutation abolished ChGroES's affinity for ChGroEL, as no binding was observed between ChGroEL and ChGroESP35T. The mutation also impacted the binding affinity with EcGroEL, as the K_d of EcGroEL-ChGroESP35T was reduced ~60-fold, to 563.0 ± 39.0 nM, compared with the K_d of EcGroEL-ChGroES. These findings confirm the importance of ChGroES P35 for interactions with the chaperonin.

In vivo complementation of *E. coli* chaperonin function. Both EcGroEL and EcGroES are required for cellular viability (33), as the chaperonin system assists in the folding of a range of essential proteins (34). To further confirm the chaperone function of ChGroEL-ChGroES and the promiscuity of the EcGroEL, we examined whether combinations of the cochaperonin/chaperonin could functionally complement EcGroEL-EcGroES using *E. coli* MGM100, which carries a conditionally lethal GroEL/GroES expression system. Based on the work of Karunakaran et al. (23) that demonstrated the failure of ChGroEL2 and ChGroEL3 to complement EcGroEL and our biochemical data supporting a molecular chaperone role for ChGroEL, complementation studies with the paralogs were not pursued. At 37°C, the chlamydial orthologs supported cell growth in a manner similar to that of the *E. coli* proteins (Fig. 4A) (also reported earlier for the *C. trachomatis* chaperonin/cochaperonin [23]), although the colonies with the chlamydial substitutions appeared less robust than the *E. coli* counterparts (Fig. 4A). However, the chlamydial system could not fully complement the *E. coli* system at 42°C (Fig. 4B), suggesting a compromised chaperone function under heat stress. Consistent with the prior report (23) and our biochemical analysis of cochaperonin/chaperonin pairings, ChGroEL required its cognate cochaperonin, ChGroES, to complement the *E. coli* chaperonin system at 37°C. By contrast, EcGroEL functioned with ChGroES in the same manner as with its cognate, EcGroES, and supported cell growth at both 37 and 42°C. These observations are consistent with the chlamydial chaperonin having a stringent

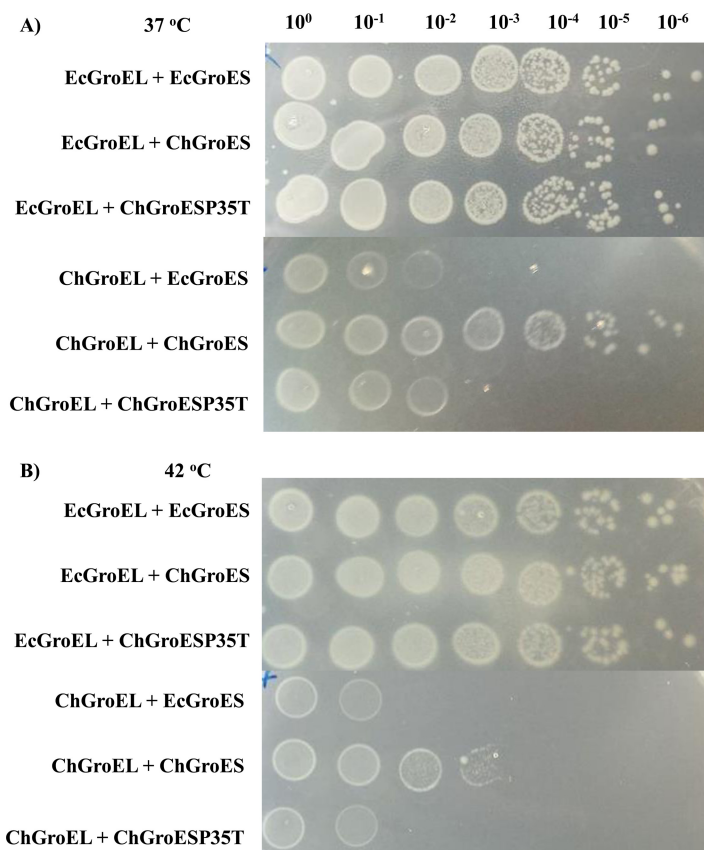


FIG 4 *In vivo* chaperone complementation assay using MGM100 at 37°C (A) and at 42°C (heat stress) (B). Cells were serially diluted and plated on LB plates containing ampicillin, kanamycin, chloramphenicol, glucose, and IPTG. The added glucose was to repress the chromosomal *EcgroEL-EcgroES* and the added IPTG was to express plasmid-carried chaperonin/cochaperonin genes controlled by the *lac* promoter in pTrc/pBbE5c or pBbE5a/pBbE5c.

requirement for its cochaperonin while the *E. coli* chaperonin can function with cochaperonin homologs.

The ability of ChGroEL-ChGroES to functionally complement EcGroEL-EcGroES at 37°C was disrupted by the P35T mutation (Fig. 4A) as predicted by our biochemical data (Table 1). However, the P35T mutation appeared not to affect chaperone function of the EcGroEL-ChGroES pairing *in vivo*, as cells expressing EcGroEL-ChGroESP35T grew as vigorously as those expressing EcGroEL-EcGroES at both 37 and 42°C. This result deviates from our biochemical observations in which the P35T mutation reduced ChGroES's effect on EcGroEL ATPase activity (Fig. 1), decreased the MDH folding rate and yield by EcGroEL-ChGroES (Fig. 2), and weakened the binding affinity for EcGroEL (Fig. 3).

Isolation and validation of *ChgroEL2* and *ChgroEL3* mutants. The results from our *in vitro* biochemical experiments and *E. coli* complementation experiments, along with prior studies, support ChGroEL as the bona fide GroEL chaperonin in *Chlamydia* (23, 35). Consequently, we hypothesized that *ChgroEL* but not *ChgroEL2* and *ChgroEL3* would be essential for chlamydial growth in cell culture. We tested this hypothesis by attempting to insertionally inactivate each *groEL* gene using a GII intron. To inactivate *ChgroEL*, *ChgroEL2*, and *ChgroEL3*, the GII intron-containing pDFTT60 vectors targeted for each *groEL* gene were separately transformed into EBs, and intron insertion mutants were selected with spectinomycin. Mutant strains carrying intron insertions in *ChgroEL2* and *ChgroEL3* were obtained using pDFTT602B and pDFTT603B, respectively, while four attempts to select mutants with two different *ChgroEL*-targeted introns failed to generate mutants. *Chlamydia* isolates harboring *ChgroEL2*::GII(*aadA*) and *ChgroEL3*::

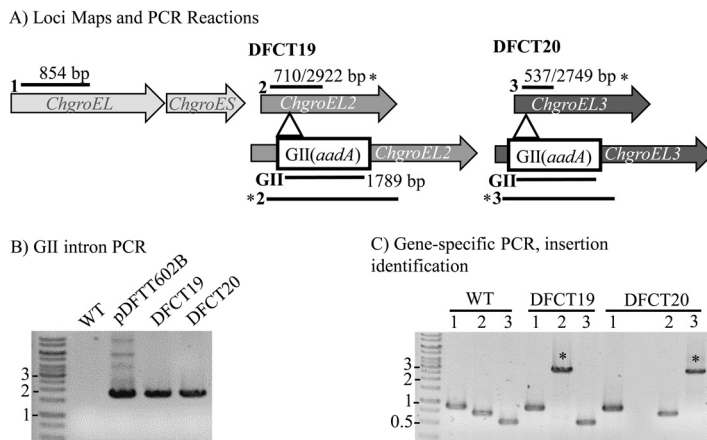


FIG 5 PCR validation of DFCT19 and DFCT20. EBs were transformed with pDFTT602B and pDFTT603B to create DFCT19 and DFCT20, respectively. Genomic DNA was isolated from both mutant strains as well as from the wild-type strain for PCR analysis. (A) Maps of the insertion sites for *ChgroEL2* and *ChgroEL3* are shown with expected PCR product sizes for the wild-type and mutated genes. (B) PCR detection of the *GII(aadA)* intron. (C) Gene-specific PCR products. Asterisks denote the mutant PCR products for *ChgroEL2* and *ChgroEL3*. Product sizes (in kilobases) are indicated by the DNA ladder. All primer sets and expected sizes are listed in Table S2 in the supplemental material.

GII(aadA) mutations were plaque purified to obtain clones DFCT19 and DFCT20, respectively.

Genomic DNA was isolated from DFCT19 and DFCT20 and used for PCR-based analysis of intron insertion (locus maps are shown in Fig. 5A). As expected, the *GII(aadA)* intron was detected in both DFCT19 and DFCT20 (Fig. 5B), and the intron insertion mapped to the expected locus, yielding PCR products approximately 2 kb larger than the wild-type genes (Fig. 5C). The PCR products from the mutant loci from DFCT19 and DFCT20 were sequenced to verify the exact locations of the intron insertions, which matched the predicted insertion sites shown in Table S2.

Gene expression analysis of DFCT19 and DFCT20. To confirm the inactivation of *ChgroEL2* and *ChgroEL3*, we used reverse transcriptase PCR to test for the loss of the gene transcripts. L2 cells were infected at a multiplicity of infection (MOI) of ~3 with DFCT19, DFCT20, or the wild-type strain, and mRNA was harvested at 30 h post-infection (PI) for cDNA synthesis. Negative-control reactions were run without reverse transcriptase to ensure the absence of contaminating genomic DNA in the cDNA preparations. All cDNA templates were assessed for the presence of *ompA* (chlamydial outer membrane protein) and *ChgroEL* transcripts as positive controls. The *ompA* and *ChgroEL* transcripts were detected in all strains (Fig. 6A and B), while the *ChgroEL2* transcript was only detected in DFCT20 and the wild-type strain (Fig. 6C) and *ChgroEL3* was detected in DFCT19 and the wild-type strain but not in DFCT20 (Fig. 6D). The absence of wild-type *ChgroEL2* and *ChgroEL3* in DFCT19 and DFCT20, respectively, is consistent with the insertional inactivation of each gene.

Growth analysis of the paralog mutants at normal and elevated temperatures. Plaque assays were initially used to determine whether DFCT19 and DFCT20 displayed growth differences compared with the wild-type parental strain. Plaques were allowed to form over 14 days, were stained with neutral red, and were assessed via light microscopy for the presence of inclusions prior to measuring. The average plaque areas for DFCT19 and DFCT20 were both significantly smaller than that of the wild-type strain (Fig. 7). No statistical difference in plaque areas was observed between DFCT19 and DFCT20.

We next explored whether the growth defect observed between the wild type and the paralog mutants was apparent over a single infection cycle, and we also explored the sensitivity of the mutants to elevated temperatures. As we hypothesized that (i) ChGroEL is the bona fide chaperonin responsible for normal protein folding and protein

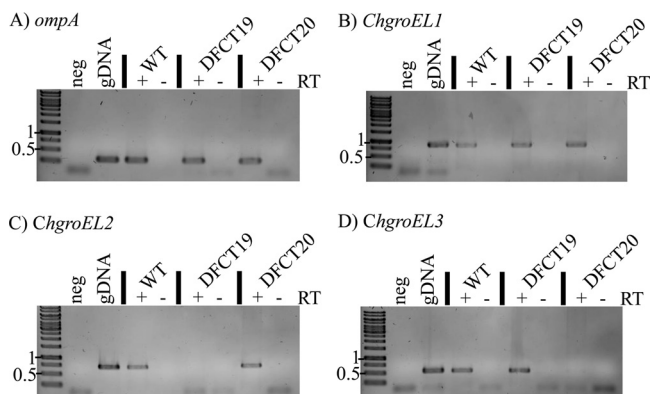


FIG 6 Gene expression analysis of DFCT19 and DFCT20. mRNA was extracted and purified from DFCT19, DFCT20, and the wild-type strain. As a negative control, one extra cDNA synthesis reaction was run per strain without the addition of reverse transcriptase. PCR was then performed to detect transcript presence. Primers specific for the chlamydial outer membrane protein gene *ompA* (A) and *ChgroEL* (B) were used as positive controls. The *ChgroEL2*-specific (C) and *ChgroEL3*-specific (D) primers were used to test for the presence of wild-type transcripts in each strain. Primer sequences and expected product sizes are listed in Table S2. Product sizes (in kilobases) are indicated by the DNA ladder. Bands lower than 0.25 kb are likely primers and were not considered.

folding under temperature stress and (ii) the paralogs perform alternative tasks, we predicted that the mutant growth deficiencies compared with the wild-type strain would not be exacerbated by heat stress. To aid in the analysis of growth phenotypes via inclusion size and progeny production, we constructed strains constitutively expressing green fluorescent protein (GFP) by transforming the DFCT19 and DFCT20 strains with pBOMB3-bla. This *E. coli-C. trachomatis* shuttle vector contains the *C. trachomatis* cryptic plasmid backbone and a *cat-gfp* fusion resulting in chloramphenicol-resistant GFP-positive strains (36). As a control, the wild-type strain was also transformed with pBOMB3-bla. The strains were plaque purified and expanded using chloramphenicol selection for the parental strain (DFCT28) and chloramphenicol and spectinomycin for the paralog mutants DFCT29 [*ChgroEL2*::GII(*aadA*)] and DFCT30 [*ChgroEL3*::GII(*aadA*)]. All subsequent growth assays were carried out using only chloramphenicol to select for the shuttle vector.

Replicate plates containing L2 cells were infected at an MOI of ~0.1 via centrifugation, and the infected cells were then incubated at either 37°C (normal temperature) or 40°C (stress temperature) for 34 h. The 40°C temperature was selected based on the

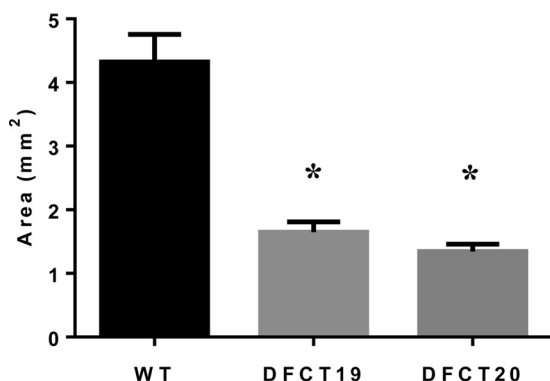


FIG 7 Analysis of DFCT19 and DFCT20 plaque phenotypes. Wild-type and mutant EBs from DFCT19 and DFCT20 were used to infect confluent monolayers of L2 cells. Cells were fed using an agarose overlay and incubated for 14 days at 37°C with 5% CO₂. Plaques were stained using neutral red and microscopically verified before plaque areas were measured. Average plaque areas in millimeters squared were calculated for each strain. Error bars represent standard errors and asterisks indicate a statistically significant difference from the wild-type strain ($P < 0.05$, one-way analysis of variance [ANOVA]). No significant differences were present between DFCT19 and DFCT20.

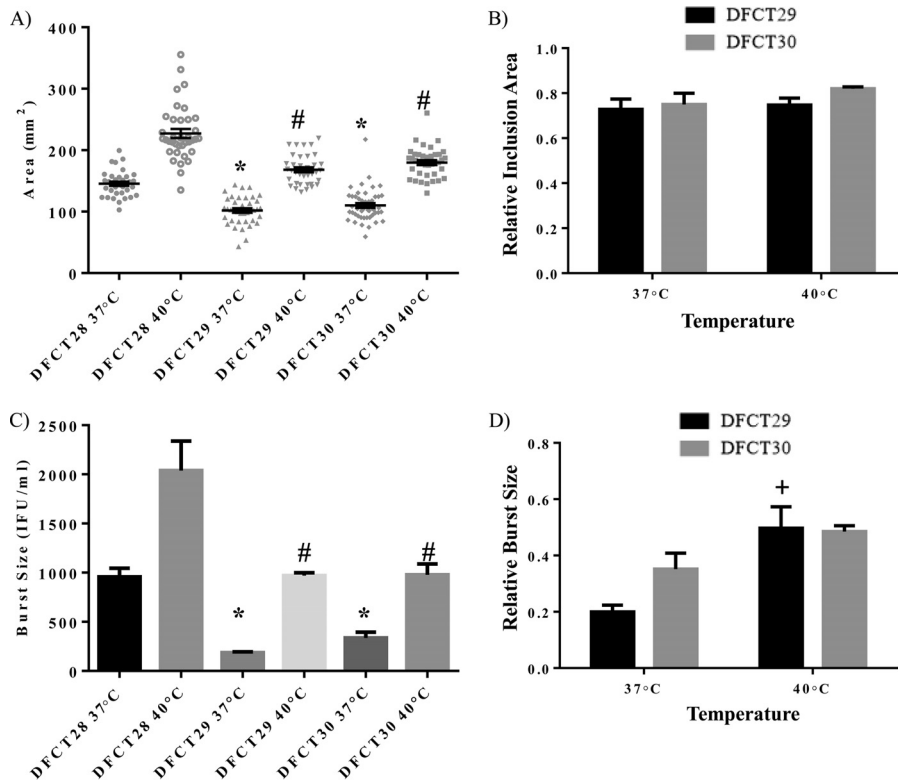


FIG 8 Growth of *ChgroEL2* and *ChgroEL3* mutants at 40°C. Strains DFCT28, DFCT29, and DFCT30 were used to infect L2 cells at an MOI of ~0.1. The infected cells were then incubated at either 37°C or 40°C for 34 h. (A) Inclusion areas were measured using ImageJ for each strain at both temperatures. (B) Relative inclusion sizes of DFCT29 and DFCT30 were calculated compared to DFCT28 at both temperatures and were not significantly different. (C) Progeny production relative to input is shown. Both mutant strains, DFCT29 and DFCT30, show significant reductions in inclusion area and burst size compared with those of the wild-type strain (DFCT28) at both temperatures. Asterisks denote a significant decrease at 37°C, while pound signs indicate a significant decrease at 40°C ($P < 0.0001$, one-way ANOVA). (D) The relative burst sizes were also calculated, showing no significant decreases at 40°C. A significant increase for DFCT29 is denoted by a plus sign ($P < 0.05$, one-way ANOVA). All experiments were performed in triplicate.

study by Brothwell et al. that identified heat-sensitive mutants from a *C. trachomatis* mutant library grown at 40°C, indicating that this temperature shift is sufficient to induce stress (37). Higher temperatures typically used for inducing a more acute stress response would likely not be sustainable for long-term culturing of the host cells (38, 39). Chlamydial growth was assessed by measuring the areas of the inclusions (Fig. 8A; see also Fig. S3) and the burst sizes (Fig. 8C) for each strain under normal and elevated temperatures. As observed with the plaque assay, both paralog mutants showed significantly reduced growth compared with that of the parental strain at both temperatures when inclusion size and progeny production were compared. However, when considering the fold reduction in growth using either metric, the growth deficiencies observed for each paralog versus the parental strain were not negatively altered by the increase in temperature (Fig. 8B and D). This is consistent with the paralogs not playing an essential role during growth under chronic high-temperature stress and supports ChGroEL as the primary chaperonin.

DISCUSSION

Despite their reduced genomes, *Chlamydia* spp. harbor and express three putative chaperonins, of which ChGroEL appears to be the bona fide chaperonin. *ChgroEL*, located in an operon with *ChgroES*, is expressed during normal growth, and its expression is upregulated during heat stress through derepression of the HrcA-CIRCE regulatory element (38, 40). Neither the *ChgroEL2* nor the *ChgroEL3* promoter encodes the CIRCE sequence recognized by HrcA, nor are the genes located next to *groES*

genes (20, 35). While ChGroEL2 levels increase during iron deprivation in cell culture, ChGroEL3 has yet to be correlated with a specific stress response (41). Interestingly, ChGroEL is antigenic in chlamydia-infected humans, and immune responses to ChGroEL have been associated with increased pathology, including tubal factor infertility (42, 43). We sought to further characterize the biochemical function of ChGroEL and to determine the essentiality of ChGroEL and its enigmatic paralogs, ChGroEL2 and ChGroEL3, for chlamydial growth under normal and temperature stress conditions to further elucidate why these reduced genome pathogens possess multiple chaperonins.

Our inability to inactivate *ChgroEL* is consistent with the predicted essentiality of this gene based on our biochemical and complementation studies and further supports its designation as the bona fide chaperonin. We also found that ChGroEL has properties distinct from those of EcGroEL. ChGroEL hydrolyzed ATP at a rate 25% of that of EcGroEL, and ChGroEL-ChGroES mediated MDH folding with slower kinetics than EcGroEL-EcGroES. In addition, ChGroEL interacted with ChGroES with a K_d six-fold lower than that for the EcGroEL-EcGroES interaction.

Importantly, we found that the chlamydial ChGroEL functions only with its cognate ChGroES but that EcGroEL is promiscuous and can function with cochaperonin homologs. The human mitochondrial chaperonin mtHsp60 has also been shown to function only with its cochaperonin, mtHsp10, and not with EcGroES, while EcGroEL can collaborate with mtHsp10 as effectively as with EcGroES in the MDH folding assay (44). Consistent with these findings, mtHsp60-EcGroES did not substitute for EcGroEL-EcGroES, while EcGroEL-mtHsp10 did in our *E. coli* complementation assays (see Fig. S2 in the supplemental material). Interestingly, EcGroEL could also function with the cochaperonin GroES from *Helicobacter pylori* (HpGroES) (Fig. S2), further supporting the promiscuity of EcGroEL. Compared with *E. coli*, which carries ~4,300 ORFs (45), intracellular *Chlamydia* and mitochondria have much-reduced proteomes, with ~900 ORFs for *Chlamydia* (20) and ~1,000 proteins found in mitochondria (46). In addition, the intracellular organisms do not possess the complete sets of proteins required for viability outside a host cell. We speculate that the cochaperonin specificity of reduced-genome organisms/organelles, particularly that of intracellular organisms, may have evolved to focus on the efficient folding of a small specialized proteome unique to their lifestyle. By contrast, the ability of the *E. coli* chaperonin to function with the cochaperonin homologs may be associated with its requirement to fold a more diverse proteome. Our results support the possibility that individual chaperonin systems have distinct properties required to maintain protein homeostasis for their host organism. Information about such distinctive chaperonin properties is important for understanding how ancient proteins such as chaperonins have been exploited by organisms to adapt to different environments and lifestyles. In addition, these distinctive chaperonin properties could be explored as organism-specific targets for therapeutics or antimicrobials. For example, because deficiencies in the human mitochondrial chaperonin system are associated with various diseases, including neurodegeneration (47), reagents specifically improving the activity of mtHsp60-mtHsp10 could be therapeutically useful.

In addition to the mechanistic adaptability of chaperonins supported by our results, chaperonins also have been shown to evolve new functions. Many bacteria contain more than one chaperonin: ~30% of bacteria whose genomes have been sequenced (189 of 669) contain chaperonin paralogs, ~21% contain one paralog, ~5.4% contain two paralogs, and one bacterium contains six paralogs (11). The best-studied chaperonin paralogs are found in mycobacteria, and these paralogs are associated with nonfolding biological functions ranging from granuloma formation (15) and biofilm maturation (16) to cell wall synthesis and oxidative stress resistance (17). In support of novel functions (48), the mycobacterial paralog appears to exist as a dimer (49), in contrast to the conventional folding-related tetradecamer (7). Limited molecular studies of paralogs from *Thermosynechococcus elongatus* and *Myxococcus xanthus* support roles in survival under temperature stress for both organisms, along with roles in predation and

development for *M. xanthus* (50, 51). Knowledge of the paralogs' novel functions not only is important for mechanistic understandings of their particular roles in the associated biological processes of the organisms but also can provide molecular insights into organism evolution. For example, the duplication and repurposed function of a chaperonin may have been necessary to meet a specific survival challenge, allowing an organism to expand into a new niche (11, 12).

In this study, we demonstrated that the chlamydial chaperonin paralogs ChGroEL2 and ChGroEL3 were not essential for *Chlamydia* under the culture conditions used, supporting the possibility that the paralogs have evolved novel functions in *Chlamydia*. In support of evolved functions, both paralogs have divergent sequences with low sequence identities (~23%) with EcGroEL, in contrast to the high sequence identity (64%) between ChGroEL and EcGroEL. Our observations that the paralog mutants generated smaller plaques and smaller inclusions and produced fewer progeny at both normal and elevated temperatures than the wild-type strain suggest that while they are not essential, both paralogs play an undefined role in chlamydial growth in cell culture. Interestingly, we saw increases in both inclusion and burst sizes for the wild-type strain and paralog mutants when incubated at 40°C compared with those at 37°C. We speculate that this difference may be due to impaired innate processes of the mouse cell line that would normally be restrictive at 37°C. However, this difference does not appear to impact the relative growth of the mutants compared with that of the wild-type strain at 37°C versus 40°C, with the exception of a slight increase in relative growth for DFCT29. In reference to paralog function, we hypothesize that the "generic" deleterious growth effects are likely to be exacerbated under non-heat-induced stress conditions. Further experiments to assess growth defects of the mutant strains under stress conditions in cell culture and using an animal model should shed light on how these proteins contribute to chlamydial biology and infection.

MATERIALS AND METHODS

Culturing of cells and bacteria. HeLa cells were used for all *C. trachomatis* transformations and plaque expansions, while L2 mouse fibroblast cells were used for plaque assays, *Chlamydia* infections destined for mRNA extraction, and temperature-sensitive growth analysis of mutants (strains are listed in Table S1 in the supplemental material) (52, 53). Cell lines were grown in Dulbecco's modified Eagle medium (DMEM) supplemented with 10% fetal bovine serum (FBS) at 37°C with 5% CO₂. For the growth of *C. trachomatis* L2 434/Bu (GenBank accession no. [NC_010287](#)), confluent cell monolayers were infected with EBs via centrifugation at 545 *g* for 1 h or by rocking for 2 h with 5% CO₂ for plaque assays. Once infected, cells were grown at 37°C with 5% CO₂ in DMEM with 10% FBS, 0.2 μ g/ml cycloheximide, and 1 nonessential amino acids. For growth of GII(*aadA*) mutant strains of *C. trachomatis*, spectinomycin was added at 500 μ g/ml, and 0.4 μ g/ml chloramphenicol was used for strains carrying pBOMB3-bla (36, 54). Assays comparing growth differences between chlamydial strains used only the antibiotics appropriate for resistance markers carried by all strains being tested. *E. coli* strain NEB 10-beta or DH5 α was used for all cloning procedures, and *E. coli* BL21(DE3) was used for protein production. *E. coli* was grown in LB broth or on LB agar containing chloramphenicol (20 or 50 μ g/ml), ampicillin (100 μ g/ml), or kanamycin (50 μ g/ml) at 30 or 37°C.

Protein expression and purification. Genes encoding ChGroEL and ChGroES were amplified from genomic DNA of *Chlamydia muridarum* strain Nigg (55) via PCR and cloned into pET15b via NcoI/BamHI and NdeI/BamHI, respectively, to express native ChGroEL and His₆-ChGroES. The ChGroESP35T mutation was generated using the QuikChange kit (Agilent). Plasmid inserts were verified using Sanger sequencing performed by the IU Center for Genomics and Bioinformatics. Conditions for cell growth, induction of protein expression, and protein purification have been described previously (24).

ATPase activity assays via malachite green. Chaperonins and cochaperonins were dialyzed into TEA reaction buffer (50 mM triethanolamine [pH 7.5], 50 mM KCl, and 20 mM MgCl₂) to final concentrations of 0.125 μ M for the tetradecameric chaperonins and 0.3 μ M for the heptameric cochaperonins. ATPase activity was measured via malachite green as previously described (24). Absorption at 660 nm (A_{660}) was measured, and the final A_{660} values were averages from three readings. The amount of hydrolyzed free phosphate was derived from a standard curve, and the hydrolysis rate was normalized to the chaperonin EcGroEL or ChGroEL monomer and expressed as the amount of PO₄ per minute per monomer. At least three independent experiments were performed.

MDH refolding assay. Chaperonins and cochaperonins were dialyzed into TEA reaction buffer. Malate dehydrogenase (MDH; Roche) was unfolded in TEA buffer including 3 M guanidine HCl to a final concentration of 36.7 μ M (monomeric MDH) for 60 min prior to the experiments. MDH refolding assays were carried out by monitoring the enzymatic activity of the refolded MDH at A_{340} (24). The final protein concentrations were 1 μ M chaperonin, 4 μ M cochaperonin, and 0.7 μ M monomeric MDH. The enzymatic activity of native MDH was set to 100%, and at least three independent experiments were performed.

Chaperonin-cochaperonin binding via MST assay. Chaperonins EcGroES, ChGroES, and ChGroESP35T were fluorescently labeled with DyLight 650 NHS ester amine-reactive dye (Thermo Fisher Scientific) according to the manufacturer's protocol. The labeled chaperonins were separated from the free dye using MidITrap (GE Healthcare) followed by dialysis (50 mM Tris HCl [pH 7.5], 100 mM KCl, 10 mM MgCl₂, and 1 mM EDTA), and the concentrations were measured using the Bradford assay. A serial dilution of 15 samples for each unlabeled protein (EcGroEL and ChGroEL) was prepared in the binding buffer (50 mM Tris HCl [pH 7.5], 100 mM KCl, 10 mM MgCl₂, 1 mM EDTA, 2 mM ADP, and 0.5 mg/ml bovine serum albumin [BSA]). Next, 10 μ l of the unlabeled protein was incubated with 10 μ l of the labeled cochaperonin for 30 min, and the solution was loaded into a glass capillary (NanoTemper Technologies) for MST measurements. The thermophoresis measurements were carried out using a NanoTemper Monolith NT115 (NanoTemper Technologies) with 80% light-emitting diode (LED) power and 40% infrared (IR) laser power. At least three independent experiments were performed. Initial MST data were processed using Monolith NT115, and the dissociation constant (K_d) was determined using KaleidaGraph by fitting the equation $y = [m1 + (m2 - m1)] / (1 + m3/x)$, where m1 is the thermophoresis reading of the labeled cochaperonin in the absence of the unlabeled titrating protein, m2 is the thermophoresis reading when all the labeled cochaperonin was bound with the unlabeled titrating protein, and m3 is the K_d .

***E. coli* MGM100 in vivo complementation assay.** *E. coli* MGM100 (kanamycin resistant) was obtained from the *E. coli* Genetic Stock Center of Yale University and grown in LB medium containing kanamycin and 0.2% arabinose, as the genomic copies of *groEL* and *groES* in MGM100 are under the control of the *ara* promoter (56). MGM100 is viable only in the presence of arabinose and is not viable in the presence of the repressor glucose. The plasmids pTrc and pBbE5a (ampicillin resistant) were used to express chaperonins EcGroEL and ChGroEL. pBbE5c (chloramphenicol resistant) was used to express cochaperonins EcGroES, ChGroES, and ChGroESP35T. These plasmids contain the *lac* promoter, and protein expression can be induced by IPTG (isopropyl- β -D-thiogalactopyranoside). Both pBbE5a and pBbE5c belong to the BglBrick series (57). CaCl₂-competent MGM100 cells were cotransformed with both plasmids and plated onto LB agar containing kanamycin, ampicillin, chloramphenicol (50 μ g/ml), and 0.2% (wt/vol) arabinose. Cultures (5 ml of LB with antibiotics and arabinose) from single colonies were grown at 37°C with shaking overnight. Culture densities were measured via optical density at 600 nm (OD₆₀₀) and adjusted to an OD₆₀₀ of 0.6. Serial dilutions (10⁻¹ to 10⁻⁷) were prepared with LB without antibiotics or arabinose, and 5 μ l of each dilution was pipetted onto LB agar containing antibiotics, 0.2% (wt/vol) glucose, and 0.1 μ M IPTG. Plates were incubated at 37°C or 42°C for 18 h.

Construction of pDFTT60 vectors. The group II intron in pDFTT3aadA was retargeted to two predicted insertion sites for *ChgroEL*, *ChgroEL2*, and *ChgroEL3* within the *C. trachomatis* L2 434/Bu genome (58) as described by Johnson and Fisher (59) using unique IBS/EBS1d/EBS2 primer sets along with the universal EBS primer. Primer sets (listed in Table S2) were used for each gene, yielding the intron donor vectors pDFTT601A, pDFTT601B, pDFTT602A, pDFTT602B, pDFTT603A, and pDFTT603B. After ligation, products were transformed into electrocompetent *E. coli* and bacteria were plated on LB agar with 20 μ g/ml chloramphenicol for selection. Recombinant vectors were isolated and the retargeted sites were verified by sequencing. DNA was routinely isolated using GeneJET DNA kits (Thermo Fisher Scientific), and Sanger DNA sequencing was performed by Macrogen USA.

Creation of ChGroEL insertion mutants. Transformation of the pDFTT60 vector series into *C. trachomatis* L2 434/Bu and mutant selection were performed as described by Lowden et al. (54). HeLa cells were used for the initial passages and expansion of plaque isolates, while L2 mouse fibroblast cells were used for plaque isolation of mutants. For all selection steps, spectinomycin was added at a concentration of 500 μ g/ml. Isolated plaques were stored in sucrose-phosphate-glutamic acid (SPG) medium and expanded in cell culture. Mutant strains DFCT19 and DFCT20 were isolated from transformations with pDFTT602B and pDFTT603B, respectively, which targeted either *ChgroEL2* or *ChgroEL3*.

Molecular validation of DFCT19 and DFCT20. Genomic DNA from DFCT19 and DFCT20 was isolated using the DNeasy blood and tissue kit (Qiagen) and was used for PCR along with Phusion high-fidelity PCR master mix. For each reaction, either 1 ng of plasmid DNA or 50 ng of genomic DNA was used as the template. The expected product sizes are listed in Table S2. PCR products were run on 1% agarose gels before being stained with ethidium bromide and were viewed via UV transillumination.

For DNA sequencing, *ChgroEL2* from DFCT19 and *ChgroEL3* from DFCT20 were amplified using the respective primer sets 60_2F/60_2R and 60_3F/60_3R and ligated into pJET1.2 from the CloneJET PCR cloning kit (Thermo Fisher Scientific). Transformants were isolated and plasmid DNA was extracted for Sanger sequencing. Inserts were sequenced using primers pJET1.2F and pJET1.2R, and sequences were analyzed in comparison to the wild-type sequence from *C. trachomatis* L2 434/Bu.

mRNA isolation and reverse transcriptase PCR. Two wells of a 24-well plate containing a confluent monolayer of L2 mouse cells were infected with either wild-type *C. trachomatis* L2 434/Bu, DFCT19, or DFCT20 EBs at an MOI of ~3 by centrifugation. At 30 h postinfection, cells were washed three times with phosphate-buffered saline (PBS) and 500 μ l of TRI reagent (Molecular Research Center) was used to harvest cell contents from each well, yielding 1-ml pooled samples. RNA extraction was performed according to the TRI reagent protocol. Extracted RNA portions were washed twice in 70% ethanol to remove excess salt and resuspended in 50 μ l of TE buffer (10 mM Tris-HCl [pH 8] with 1 mM EDTA). Host cell RNA and rRNAs were removed using the MICROBEnrich and MICROBExpress kits (Ambion), and purified RNA was resuspended in 50 μ l of nuclease free water. The random hexamer primer protocol of the Maxima H Minus First Strand cDNA synthesis kit with double-strand-specific DNase (dsDNase) (Thermo Fisher Scientific) was then used to synthesize cDNA. For each RNA sample, two reaction mixtures were set up containing either reverse transcriptase or water as a control. PCR was performed using

Fermentas 2⁺ master mix (Thermo Fisher Scientific) in 50- μ l reaction mixtures containing 2 μ l of each cDNA reaction product as the template. Primer sets 60_1F/60_1R, 60_2F/60_2R, 60_3F/60_3R, and FPompA/RPompA were used to amplify each sample over 30 cycles, and 10 μ l of each PCR product was separated on 1% agarose gels before ethidium bromide staining and viewing via UV transillumination.

C. trachomatis plaque assay phenotype analysis. Confluent L2 mouse cells in 60-mm cell culture dishes were infected with \sim 20 EBs of either the wild type, DFCT19, or DFCT20 by rocking for 1 h at 37°C or for 2 h at 37°C with 5% CO₂. The medium was replaced with an agarose overlay and plaque dishes were fed with fresh agarose overlays at 5-day intervals. Plaques were then stained with neutral red after 14 days of incubation and verified using light microscopy, and plaque dimensions were measured with a hand loupe. Plaque areas were calculated and the average plaque area was determined for each strain. All assays were performed in the absence of spectinomycin.

Growth of chlamydial strains at an elevated temperature. To facilitate the assessment of any growth differences among the wild type and the mutant chlamydial strains at an elevated temperature, strains carrying a GFP-producing vector were constructed. The pBOMB3 vector (kindly provided by Ted Hackstadt) (36) was modified via removal of the *bla* resistance cassette using inverse PCR and primers BOMB3-blaF and BOMB3-blaR. Briefly, PCR was performed using Phusion high-fidelity polymerase and the PCR product was gel purified and self-ligated. Ligation products were transformed into NEB 10-beta *E. coli*, and transformants were selected with chloramphenicol at 20 μ g/ml. The pBOMB3-bla plasmid was then isolated and sequenced in its entirety to ensure that no errors were introduced into the cryptic plasmid backbone and shuttle region of the vector during PCR. The vector was then transformed into the parental strain and the *ChgroEL2* and *ChgroEL3* mutants, DFCT19 and DFCT20, respectively, using our transformation protocol and the chloramphenicol selection protocol described by Weber et al. (36) except that chloramphenicol was used at 0.4 μ g/ml starting at passage 3 instead of passage 4. The resulting strains, DFCT28 (parental background), DFCT29 (DFCT19 background), and DFCT30 (DFCT20 background), were plaque purified and expanded, and we determined the titers using the inclusion-forming unit (IFU) assay (53) with vector-encoded GFP fluorescence as an inclusion marker.

Confluent L2 cells in 96-well plates were infected at an MOI of \sim 0.1 with DFCT28, DFCT29, or DFCT30 via centrifugation at 545 g for 1 h using medium supplemented with chloramphenicol at 0.4 μ g/ml. Duplicate plates were then incubated for 1 h at 37°C with 5% CO₂ before being incubated at either 37°C or 40°C with 5% CO₂. At 34 h postinfection, fluorescent inclusions were imaged at \times 400 magnification using a Leica DMIL microscope fitted with a Leica EC4 camera and LAS EZ software (Leica). The cross-sectional areas of inclusions were measured using ImageJ (freeware from <https://www.nih.gov/>) for at least 95 inclusions per strain. Progeny were then harvested from the wells, and the IFU assay was performed to measure infectious EBs. All experiments were performed in triplicate with three technical replicates used per type for each assay.

SUPPLEMENTAL MATERIAL

Supplemental material for this article may be found at <https://doi.org/10.1128/JB.00844-16>.

SUPPLEMENTAL FILE 1, PDF file, 1.3 MB.

ACKNOWLEDGMENTS

We thank Evan Landers and Charlotte Key for their assistance with vector and strain construction.

Research in the Chen laboratory was partly supported by the Indiana Clinical and Translational Sciences Institute, which is funded in part by grant number UL1TR001108 from the National Institutes of Health, National Center for Advancing Translational Sciences, Clinical and Translational Sciences Award. The Chen laboratory also acknowledges a research fund from the Department of Molecular and Cellular Biochemistry, Indiana University. Work by the Fisher lab was supported by the NIAID of the National Institutes of Health under award number 1R21AI115238-01 to D.J.F.

The content is solely the responsibility of the authors and does not necessarily represent the official views of the National Institutes of Health.

REFERENCES

- Gupta RS. 1996. Evolutionary relationships of chaperonins, p 27–64. In Ellis RJ (ed), *The chaperonins*. Academic Press, Inc., San Diego, CA.
- Brocchieri L, Karlin S. 2000. Conservation among HSP60 sequences in relation to structure, function, and evolution. *Protein Sci* 9:476–486. <https://doi.org/10.1110/ps.9.3.476>.
- Sigler PB, Xu Z, Rye HS, Burston SG, Fenton WA, Horwich AL. 1998. Structure and function in GroEL-mediated protein folding. *Annu Rev Biochem* 67:581–608. <https://doi.org/10.1146/annurev.biochem.67.1.581>.
- Thirumalai D, Lorimer GH. 2001. Chaperonin-mediated protein folding. *Annu Rev Biophys Biomol Struct* 30:245–269. <https://doi.org/10.1146/annurev.biophys.30.1.245>.
- Lin Z, Rye HS. 2006. GroEL-mediated protein folding: making the impossible, possible. *Crit Rev Biochem Mol Biol* 41:211–239. <https://doi.org/10.1080/10409230600760382>.
- Horwich AL, Farr GW, Fenton WA. 2006. GroEL-GroES-mediated protein folding. *Chem Rev* 106:1917–1930. <https://doi.org/10.1021/cr040435v>.
- Braig K, Otwinowski Z, Hegde R, Boisvert DC, Joachimiak A, Horwich AL, Sigler PB. 1994. The crystal structure of the bacterial chaperonin GroEL at 2.8 Å. *Nature* 371:578–586. <https://doi.org/10.1038/371578a0>.

8. Hunt JF, Weaver AJ, Landry SJ, Gierasch L, Deisenhofer J. 1996. The crystal structure of the GroES co-chaperonin at 2.8 Å resolution. *Nature* 379:37–45. <https://doi.org/10.1038/379037a0>.
9. Mande SC, Mehra V, Bloom BR, Hol WG. 1996. Structure of the heat shock protein chaperonin-10 of *Mycobacterium leprae*. *Science* 271:203–207. <https://doi.org/10.1126/science.271.5246.203>.
10. Xu Z, Horwich AL, Sigler PB. 1997. The crystal structure of the asymmetric GroEL-GroES-(ADP)₇ chaperonin complex. *Nature* 388:741–750. <https://doi.org/10.1038/41944>.
11. Lund PA. 2009. Multiple chaperonins in bacteria—why so many? *FEMS Microbiol Rev* 33:785–800. <https://doi.org/10.1111/j.1574-6976.2009.00178.x>.
12. Henderson B, Fares MA, Lund PA. 2013. Chaperonin 60: a paradoxical, evolutionarily conserved protein family with multiple moonlighting functions. *Biol Rev Camb Philos Soc* 88:955–987. <https://doi.org/10.1111/brv.12037>.
13. Rinke de Wit TF, Bekelie S, Osland A, Miko TL, Hermans PW, van Soolingen D, Drijfhout JW, Schoninger R, Janson AA, Thole JE. 1992. *Mycobacterium tuberculosis* contains two *groEL* genes: the second *Mycobacterium leprae* *groEL* gene is arranged in an operon with *groES*. *Mol Microbiol* 6:1995–2007. <https://doi.org/10.1111/j.1365-2958.1992.tb01372.x>.
14. Kong TH, Coates AR, Butcher PD, Hickman CJ, Shinnick TM. 1993. *Mycobacterium tuberculosis* expresses two chaperonin-60 homologs. *Proc Natl Acad Sci U S A* 90:2608–2612. <https://doi.org/10.1073/pnas.90.7.2608>.
15. Hu Y, Henderson B, Lund PA, Tormay P, Ahmed MT, Gurcha SS, Besra GS, Coates AR. 2008. A *Mycobacterium tuberculosis* mutant lacking the *groEL* homologue *cpn60.1* is viable but fails to induce an inflammatory response in animal models of infection. *Infect Immun* 76:1535–1546. <https://doi.org/10.1128/IAI.01078-07>.
16. Ojha A, Anand M, Bhatt A, Kremer L, Jacobs WR, Jr, Hatfull GF. 2005. GroEL1: a dedicated chaperone involved in mycolic acid biosynthesis during biofilm formation in mycobacteria. *Cell* 123:861–873. <https://doi.org/10.1016/j.cell.2005.09.012>.
17. Wang XM, Lu C, Soetaert K, S'Heeren C, Peirs P, Laneelle MA, Lefevre P, Bifani P, Content J, Daffe M, Huygen K, De Bruyn J, Wattiez R. 2011. Biochemical and immunological characterization of a *cpn60.1* knockout mutant of *Mycobacterium bovis* BCG. *Microbiology* 157:1205–1219. <https://doi.org/10.1099/mic.0.045120-0>.
18. Centers for Disease Control and Prevention. Chlamydia- CDC fact sheet. Centers for Disease Control and Prevention, Atlanta, GA. <http://www.cdc.gov/std/chlamydia/Stdfact-chlamydia.htm>.
19. Abdelrahman YM, Belland RJ. 2005. The chlamydial developmental cycle. *FEMS Microbiol Rev* 29:949–959. <https://doi.org/10.1016/j.femsre.2005.03.002>.
20. Stephens RS, Kalman S, Lammel C, Fan J, Marathe R, Aravind L, Mitchell W, Olinger L, Tatusov RL, Zhao Q, Koonin EV, Davis RW. 1998. Genome sequence of an obligate intracellular pathogen of humans: *Chlamydia trachomatis*. *Science* 282:754–759. <https://doi.org/10.1126/science.282.5389.754>.
21. Voigt A, Schofl G, Saluz HP. 2012. The *Chlamydia psittaci* genome: a comparative analysis of intracellular pathogens. *PLoS One* 7:e35097. <https://doi.org/10.1371/journal.pone.0035097>.
22. Okuda H, Sakuhana C, Yamamoto R, Mizukami Y, Kawai R, Sumita Y, Koga M, Shirai M, Matsuda K. 2008. The intermediate domain defines broad nucleotide selectivity for protein folding in *Chlamydomonas* GroEL1. *J Biol Chem* 283:9300–9307. <https://doi.org/10.1074/jbc.M710057200>.
23. Karunakaran KP, Noguchi Y, Read TD, Cherkasov A, Kwee J, Shen C, Nelson CC, Brunham RC. 2003. Molecular analysis of the multiple GroEL proteins of *Chlamydiae*. *J Bacteriol* 185:1958–1966. <https://doi.org/10.1128/JB.185.6.1958-1966.2003>.
24. Illingworth M, Ramsey A, Zheng Z, Chen L. 2011. Stimulating the substrate folding activity of a single ring GroEL variant by modulating the cochaperonin GroES. *J Biol Chem* 286:30401–30408. <https://doi.org/10.1074/jbc.M111.255935>.
25. Chandrasekhar GN, Tilly K, Woolford C, Hendrix R, Georgopoulos C. 1986. Purification and properties of the *groES* morphogenetic protein of *Escherichia coli*. *J Biol Chem* 261:12414–12419.
26. Jackson GS, Staniforth RA, Halsall DJ, Atkinson T, Holbrook JJ, Clarke AR, Burston SG. 1993. Binding and hydrolysis of nucleotides in the chaperonin catalytic cycle: implications for the mechanism of assisted protein folding. *Biochemistry* 32:2554–2563. <https://doi.org/10.1021/bi00061a013>.
27. Todd MJ, Viitanen PV, Lorimer GH. 1994. Dynamics of the chaperonin ATPase cycle: implications for facilitated protein folding. *Science* 265:659–666. <https://doi.org/10.1126/science.7913555>.
28. Illingworth M, Salisbury J, Li W, Lin D, Chen L. 2015. Effective ATPase activity and moderate chaperonin-cochaperonin interaction are important for the functional single-ring chaperonin system. *Biochem Biophys Res Commun* 466:15–20. <https://doi.org/10.1016/j.bbrc.2015.08.034>.
29. Landry SJ, Taher A, Georgopoulos C, van der Vies SM. 1996. Interplay of structure and disorder in cochaperonin mobile loops. *Proc Natl Acad Sci U S A* 93:11622–11627. <https://doi.org/10.1073/pnas.93.21.11622>.
30. Ben-Zvi AP, Chatellier J, Fersht AR, Goloubinoff P. 1998. Minimal and optimal mechanisms for GroE-mediated protein folding. *Proc Natl Acad Sci U S A* 95:15275–15280. <https://doi.org/10.1073/pnas.95.26.15275>.
31. Todd MJ, Viitanen PV, Lorimer GH. 1993. Hydrolysis of adenosine 5'-triphosphate by *Escherichia coli* GroEL: effects of GroES and potassium ion. *Biochemistry* 32:8560–8567. <https://doi.org/10.1021/bi00084a024>.
32. Kovalenko O, Yifrach O, Horovitz A. 1994. Residue lysine-34 in GroES modulates allosteric transitions in GroEL. *Biochemistry* 33:14974–14978. <https://doi.org/10.1021/bi00254a004>.
33. Fayet O, Ziegelhoffer T, Georgopoulos C. 1989. The *groES* and *groEL* heat shock gene products of *Escherichia coli* are essential for bacterial growth at all temperatures. *J Bacteriol* 171:1379–1385. <https://doi.org/10.1128/jb.171.3.1379-1385.1989>.
34. Houry WA, Frishman D, Eckerskorn C, Lottspeich F, Hartl FU. 1999. Identification of *in vivo* substrates of the chaperonin GroEL. *Nature* 402:147–154. <https://doi.org/10.1038/45977>.
35. McNally D, Fares MA. 2007. *In silico* identification of functional divergence between the multiple *groEL* gene paralogs in *Chlamydiae*. *BMC Evol Biol* 7:81. <https://doi.org/10.1186/1471-2148-7-81>.
36. Weber MM, Noriega NF, Bauler LD, Lam JL, Sager J, Wesolowski J, Paumet F, Hackstadt T. 2016. A functional core of IncA is required for *Chlamydia trachomatis* inclusion fusion. *J Bacteriol* 198:1347–1355. <https://doi.org/10.1128/JB.00933-15>.
37. Brothwell JA, Muramatsu MK, Toh E, Rockey DD, Putman TE, Barta ML, Hefty PS, Suchland RJ, Nelson DE. 2016. Interrogating genes that mediate *Chlamydia trachomatis* survival in cell culture using conditional mutants and recombination. *J Bacteriol* 198:2131–2139. <https://doi.org/10.1128/JB.00161-16>.
38. Hanson BR, Tan M. 2015. Transcriptional regulation of the *Chlamydia* heat shock stress response in an intracellular infection. *Mol Microbiol* 97:1158–1167. <https://doi.org/10.1111/mmi.13093>.
39. Huston WM, Theodoropoulos C, Mathews SA, Timms P. 2008. *Chlamydia trachomatis* responds to heat shock, penicillin induced persistence, and IFN-gamma persistence by altering levels of the extracytoplasmic stress response protease HtrA. *BMC Microbiol* 8:190. <https://doi.org/10.1186/1471-2180-8-190>.
40. Wilson AC, Wu CC, Yates JR, III, Tan M. 2005. Chlamydial GroEL autoregulates its own expression through direct interactions with the HrcA repressor protein. *J Bacteriol* 187:7535–7542. <https://doi.org/10.1128/JB.187.21.7535-7542.2005>.
41. LaRue RW, Dill BD, Giles DK, Whittimore JD, Raulston JE. 2007. Chlamydial Hsp60-2 is iron responsive in *Chlamydia trachomatis* serovar E-infected human endometrial epithelial cells *in vitro*. *Infect Immun* 75:2374–2380. <https://doi.org/10.1128/IAI.01465-06>.
42. Hjelholt A, Christiansen G, Johannesson TG, Ingerslev HJ, Birkelund S. 2011. Tubal factor infertility is associated with antibodies against *Chlamydia trachomatis* heat shock protein 60 (HSP60) but not human HSP60. *Hum Reprod* 26:2069–2076. <https://doi.org/10.1093/humrep/der167>.
43. Tiitinen A, Surcel HM, Halttunen M, Birkelund S, Bloigu A, Christiansen G, Koskela P, Morrison SG, Morrison RP, Paavonen J. 2006. *Chlamydia trachomatis* and chlamydial heat shock protein 60-specific antibody and cell-mediated responses predict tubal factor infertility. *Hum Reprod* 21:1533–1538. <https://doi.org/10.1093/humrep/del014>.
44. Parnas A, Nisemblat S, Weiss C, Levy-Rimler G, Pri-Or A, Zor T, Lund PA, Bross P, Azem A. 2012. Identification of elements that dictate the specificity of mitochondrial Hsp60 for its co-chaperonin. *PLoS One* 7:e50318. <https://doi.org/10.1371/journal.pone.0050318>.
45. Blattner FR, Plunkett G, III, Bloch CA, Perna NT, Burland V, Riley M, Collado-Vides J, Glasner JD, Rode CK, Mayhew GF, Gregor J, Davis NW, Kirkpatrick HA, Goeden MA, Rose DJ, Mau B, Shao Y. 1997. The complete genome sequence of *Escherichia coli* K-12. *Science* 277:1453–1462. <https://doi.org/10.1126/science.277.5331.1453>.
46. Fox TD. 2012. Mitochondrial protein synthesis, import, and assembly. *Genetics* 192:1203–1234. <https://doi.org/10.1534/genetics.112.141267>.
47. Bross P, Magnoni R, Bie AS. 2012. Molecular chaperone disorders: de-

- fective Hsp60 in neurodegeneration. *Curr Top Med Chem* 12:2491–2503. <https://doi.org/10.2174/1568026611212220005>.
48. Fan M, Rao T, Zacco E, Ahmed MT, Shukla A, Ojha A, Freeke J, Robinson CV, Benesch JL, Lund PA. 2012. The unusual mycobacterial chaperonins: evidence for *in vivo* oligomerization and specialization of function. *Mol Microbiol* 85:934–944. <https://doi.org/10.1111/j.1365-2958.2012.08150.x>.
49. Qamra R, Srinivas V, Mande SC. 2004. *Mycobacterium tuberculosis* GroEL homologues unusually exist as lower oligomers and retain the ability to suppress aggregation of substrate proteins. *J Mol Biol* 342:605–617. <https://doi.org/10.1016/j.jmb.2004.07.066>.
50. Li J, Wang Y, Zhang CY, Zhang WY, Jiang DM, Wu ZH, Liu H, Li YZ. 2010. *Myxococcus xanthus* viability depends on *groEL* supplied by either of two genes, but the paralogs have different functions during heat shock, predation, and development. *J Bacteriol* 192:1875–1881. <https://doi.org/10.1128/JB.01458-09>.
51. Sato S, Ikeuchi M, Nakamoto H. 2008. Expression and function of a *groEL* paralog in the thermophilic cyanobacterium *Thermosynechococcus elongatus* under heat and cold stress. *FEBS Lett* 582:3389–3395. <https://doi.org/10.1016/j.febslet.2008.08.034>.
52. Banks J, Eddie B, Schachter J, Meyer KF. 1970. Plaque formation by *Chlamydia* in L cells. *Infect Immun* 1:259–262.
53. Scidmore MA. 2005. Cultivation and laboratory maintenance of *Chlamydia trachomatis*. *Curr Protoc Microbiol* Chapter 11:Unit 11A.1. <https://doi.org/10.1002/9780471729259.mc11a01s00>.
54. Lowden NM, Yeruva L, Johnson CM, Bowlin AK, Fisher DJ. 2015. Use of aminoglycoside 3' adenylyltransferase as a selection marker for *Chlamydia trachomatis* intron-mutagenesis and *in vivo* intron stability. *BMC Res Notes* 8:570. <https://doi.org/10.1186/s13104-015-1542-9>.
55. Read TD, Brunham RC, Shen C, Gill SR, Heidelberg JF, White O, Hickey EK, Peterson J, Utterback T, Berry K, Bass S, Linher K, Weidman J, Khouri H, Craven B, Bowman C, Dodson R, Gwinn M, Nelson W, DeBoy R, Kolonay J, McClarty G, Salzberg SL, Eisen J, Fraser CM. 2000. Genome sequences of *Chlamydia trachomatis* MoPn and *Chlamydia pneumoniae* AR39. *Nucleic Acids Res* 28:1397–1406. <https://doi.org/10.1093/nar/28.6.1397>.
56. McLennan N, Masters M. 1998. GroE is vital for cell-wall synthesis. *Nature* 392:139. <https://doi.org/10.1038/32317>.
57. Lee TS, Krupa RA, Zhang F, Hajimorad M, Holtz WJ, Prasad N, Lee SK, Keasling JD. 2011. BglBrick vectors and datasheets: a synthetic biology platform for gene expression. *J Biol Eng* 5:12. <https://doi.org/10.1186/1754-1611-5-12>.
58. Thomson NR, Holden MT, Carder C, Lennard N, Lockey SJ, Marsh P, Skipp P, O'Connor CD, Goodhead I, Norbertzack H, Harris B, Ormond D, Rance R, Quail MA, Parkhill J, Stephens RS, Clarke IN. 2008. *Chlamydia trachomatis*: genome sequence analysis of lymphogranuloma venereum isolates. *Genome Res* 18:161–171. <https://doi.org/10.1101/gr.7020108>.
59. Johnson CM, Fisher DJ. 2013. Site-specific, insertional inactivation of *incA* in *Chlamydia trachomatis* using a group II intron. *PLoS One* 8:e83989. <https://doi.org/10.1371/journal.pone.0083989>.